



HAL
open science

Thermal evolution of hydrated asteroids inferred from oxygen isotopes

Lionel Vacher, Maxime Piralla, Matthieu Gounelle, Martin Bizzarro, Yves Marrocchi

► **To cite this version:**

Lionel Vacher, Maxime Piralla, Matthieu Gounelle, Martin Bizzarro, Yves Marrocchi. Thermal evolution of hydrated asteroids inferred from oxygen isotopes. *The Astrophysical journal letters*, 2019, 882, pp.L20. 10.3847/2041-8213/ab3bd0 . hal-02331795

HAL Id: hal-02331795

<https://hal.univ-lorraine.fr/hal-02331795>

Submitted on 24 Oct 2019

HAL is a multi-disciplinary open access archive for the deposit and dissemination of scientific research documents, whether they are published or not. The documents may come from teaching and research institutions in France or abroad, or from public or private research centers.

L'archive ouverte pluridisciplinaire **HAL**, est destinée au dépôt et à la diffusion de documents scientifiques de niveau recherche, publiés ou non, émanant des établissements d'enseignement et de recherche français ou étrangers, des laboratoires publics ou privés.



Distributed under a Creative Commons Attribution 4.0 International License

1 **Thermal evolution of hydrated asteroids inferred from oxygen isotopes**

2
3
4
5 Lionel G. Vacher^{1,2,*}, Maxime Piralla¹, Matthieu Gounelle³, Martin Bizzarro⁴ & Yves
6 Marrocchi¹

7
8
9 ¹CRPG, CNRS, Université de Lorraine, UMR 7358, Vandoeuvre les Nancy, F-54501, France

10
11 ²Department of Physics, Washington University, St. Louis, MO, USA

12
13 ³IMPMC, MNHN, UPMC, UMR CNRS 7590, 61 rue Buffon, 75005 Paris, France

14
15 ⁴Centre for Star and Planet Formation and Natural History Museum of Denmark, University
16 of Copenhagen, DK-1350 Copenhagen, Denmark

17
18 * corresponding author: l.vacher@wustl.edu

19
20
21
22
23
24
25
26
27
28
29
30
31
32
33
34
35
36
37
38
39
40
41
42
43
44
45
46
47
48
49
50
51
52

53 **Abstract**

54

55 Chondrites are fragments of unmelted asteroids that formed due to gravitational
56 instabilities in turbulent regions of the Solar protoplanetary disk. Hydrated chondrites are
57 common among meteorites, indicating that a substantial fraction of the rocky bodies that
58 formed early in the Solar System accreted water ice grains that subsequently melted due to
59 heat released by the radioactive decay of ^{26}Al . However, the thermal histories of asteroids are
60 still largely unknown whereas it would bring fundamental information on their timing of
61 accretion and their physical characteristics. Here we show that hydrated meteorites (CM
62 chondrites) contain previously uncharacterized calcium carbonates with peculiar oxygen
63 isotopic compositions ($\Delta^{17}\text{O} \approx -2.5 \text{‰}$), which artificially produce the mass-independent trend
64 previously reported for carbonates. Based on these isotopic data, we propose a new model to
65 quantitatively estimate the precipitation temperatures of secondary phases (carbonates and
66 serpentine). It reveals that chondritic secondary phases recorded a gradual increase of the
67 temperature during the extent of aqueous alteration, from -10 °C to maximum 250 °C . We
68 also show that the thermal path of C-type asteroids is independent of the initial oxygen
69 isotopic composition of the primordial water ice grains that they accreted. Our estimated
70 temperatures for hydrated asteroids remain lower than those experienced by other
71 carbonaceous chondrites, providing strong constraints for modelling the formation conditions
72 and size-distribution of water-rich asteroids, especially in anticipation of the return of samples
73 of water-rich asteroids to Earth by the OSIRIS-REx and Hayabusa2 missions.

74 **1. Introduction**

75

76 Dark C-type asteroids dominate the main-belt asteroid population and are genetically
77 related to hydrous primitive CI and CM carbonaceous chondrites (Vilas & Gaffey 1989; Hiroi
78 et al. 1996; Vilas 1994; Burbine et al. 2002; Lauretta et al. 2019). CM chondrites are the most
79 common water-rich meteorites, and CM-like matter represent an important fraction of
80 exogenic clasts reported in other groups of meteorites, implying that CM parent bodies are
81 widespread in the asteroid belt (Briani et al. 2012). CM chondrites are complex aggregates of
82 high-temperature components formed in the disk and low-temperature secondary minerals
83 formed during subsequent parent-body fluid circulations. The latter provide key constraints
84 on the origin of water accreted by asteroids (Vacher et al. 2016; Piani et al. 2018) as well as
85 their accretion and evolution histories (Young et al. 2003; Verdier-Paoletti et al. 2017; Vacher
86 et al. 2017; Fujiya et al. 2015). CM chondrites are therefore important samples because they
87 show varying degrees of alteration that can be easily estimated by their chemical alteration
88 index (Rubin et al. 2007; Marrocchi et al. 2014; Vacher et al. 2018). Among secondary
89 minerals, carbonates are of primary importance as they represent direct proxies of the
90 asteroidal fluids from which they formed and can, in theory, be used to decipher their thermal
91 evolution (Clayton & Mayeda 1984). However, determining carbonate precipitation
92 temperatures requires knowledge of the O isotopic compositions of their parental fluids,
93 which itself requires knowledge of the carbonate precipitation temperatures, leading to a
94 seemingly circular problem.

95 The temperature of CM carbonate precipitation remains largely underconstrained and
96 proposed values cover a large range of temperatures. More generally, the sequence of
97 formation of the different secondary phases (carbonates, serpentine) is poorly understood.
98 Based on ‘clumped-isotopes’ and oxygen isotopic analyses, it has been proposed that CM

99 carbonates could have precipitated at both low and medium temperatures, in the range of 0-
100 75°C (Clayton & Mayeda 1984; Benedix et al. 2003; Guo & Eiler 2007) and 50-350°C
101 (Verdier-Paoletti et al. 2017; Alexander et al. 2015). However, these two different
102 methodologies do not take account the petrographic relationship between carbonates and
103 serpentine (Fuchs et al. 1973; Zolensky et al. 1997; Brearley 2006; Rubin et al. 2007; Vacher
104 et al. 2018; Lee et al. 2013; 2014), which can constrain the evolution of the fluid over time. In
105 addition, different types of carbonates are present in CM chondrites (Vacher et al. 2017; Lee
106 et al. 2013; 2014) but no specific attention has been paid on their respective oxygen isotopic
107 compositions. The objectives of this paper are thus to determine the oxygen isotopic
108 composition of petrographically characterized carbonates in order to quantify the thermal
109 evolution of hydrated asteroids. To do so, we surveyed a suite of different CM chondrites
110 characterized by varying degrees of alteration: CM2.6/2.7 Maribo (van Kooten et al. 2018),
111 CM2.5 Murchison (Rubin et al. 2007), CM2.4/2.7 Jbilet Winselwan (King et al. 2018) and
112 CM2.0 Mukundpura (Rudraswami et al. 2018). Based on oxygen isotopic compositions of
113 carbonates, we propose a new isotopic alteration model that reconciles petrographic
114 observations and formation temperatures of CM carbonates.

115

116 **2. Material and methods**

117 *2.1 SEM imaging*

118 Calcite grains were located in carbon coated (i) polished sections of Murchison,
119 Mukundpura and Jbilet Winselwan (samples provided by the Muséum National d'Histoire
120 Naturelle in Paris) and (ii) thin section of Maribo (section provided by the Natural History
121 Museum of Denmark in Copenhagen) using a Scanning Electron Microscope (SEM) JEOL
122 JSM-6510 equipped with an energy dispersive X-ray detector (Bruker-AXS XFlash, silicon
123 drift detector) at Centre de Recherches Pétrographiques et Géochimiques (CRPG, Nancy,

124 France). Back-Scattered Electron (BSE) imaging were performed with a 3 nA electron beam
125 current operated at 15 kV.

126

127 *2.2 SIMS oxygen isotope analyses of calcite*

128 Calcite oxygen isotopic compositions were analysed using a CAMECA IMS 1270 E7 at
129 CRPG laboratory. A Cs⁺ primary ion beam (~15x10 μm spot area) with a current of ~5 nA
130 was used in order to collect ¹⁶O⁻, ¹⁷O⁻ and ¹⁸O⁻ secondary ions in multi-collection mode using
131 three Faraday cups (L'2, FC2 and H1). Charge compensation was applied using a normal-
132 incidence electron gun. Mass Resolving Power (MRP = M/ΔM) was adjusted to ~7000 to
133 resolve interference from ¹⁶OH⁻ on the ¹⁷O⁻ peak and achieve maximum flatness on the top of
134 the ¹⁶O⁻ and ¹⁸O⁻ peaks (entrance and exit slits of FC2 were adjusted to ~70 μm and ~170 μm,
135 respectively). ¹⁶O⁻ and ¹⁸O⁻ secondary ions were collected on L'2 and H1, respectively (slit 1,
136 MRP ≈ 2500). Pre-sputter on a large area (~20x20 μm) was applied before each measurement
137 during 60s in order to remove carbon coating at the surface of the calcite grains. Acquisition
138 time was set to ~5s and measurements were repeated over 30 cycles to achieve counting
139 statistics ~0.2‰ (1σ) for δ¹⁸O and ~0.3‰ for δ¹⁷O. Isotope ratios (¹⁷O/¹⁶O and ¹⁸O/¹⁶O) are
140 presented in per mil (‰) relative to Standard Mean Ocean Water (SMOW):

$$141 \quad \delta^x\text{O}_{SMOW}(\text{‰}) = \left(\frac{x\text{O}/^{16}\text{O}_{sample}}{x\text{O}/^{16}\text{O}_{SMOW}} - 1 \right) \times 1000 \quad (1)$$

142 where x represents ¹⁷O or ¹⁸O and SMOW the ratios of the SMOW standard. We measured
143 two in-house terrestrial standards to define the Terrestrial Fractionation Line (TFL): (i) quartz
144 (SiO₂) from Brazil (δ¹⁸O = 9.6‰, ¹⁶O = 2 × 10⁹ cps and ¹⁸O = 4.2 × 10⁶ cps) and (ii) calcite
145 (CaCO₃) from Mexico (δ¹⁸O = 23.6‰, ¹⁶O = 2 × 10⁹ cps and ¹⁸O = 4.2 × 10⁶ cps; 0.03 wt% of
146 MgO). Instrumental Mass Fractionation (IMF) for calcite matrix was determined from our in-
147 house Mexican calcite standard at the beginning and end of each analytical session. IMF
148 values for each sample analysis were then calculated by accounting for the linear deviation

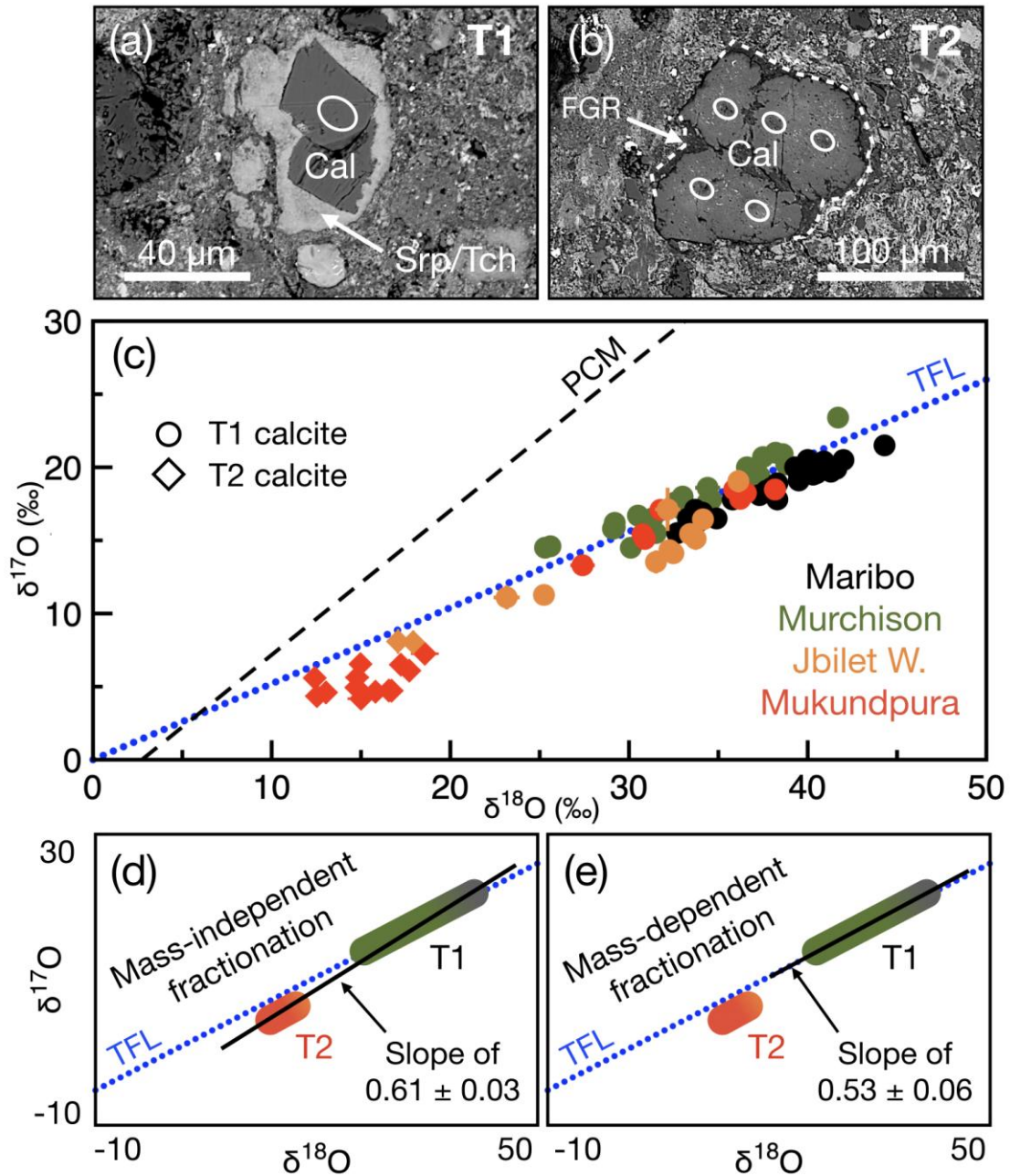
149 over the time of the IMF values. Typical measurement errors (2σ), accounting for errors on
150 each measurement and the external reproducibility of the standard, were estimated to be
151 $\sim 0.5\text{‰}$ for $\delta^{18}\text{O}$, $\sim 0.6\text{‰}$ for $\delta^{17}\text{O}$, and $\sim 0.7\text{‰}$ for $\Delta^{17}\text{O}$ (i.e., $\Delta^{17}\text{O} = \delta^{17}\text{O} - 0.52 \times \delta^{18}\text{O}$),
152 where $\Delta^{17}\text{O}$ represents the departure from the TFL.

153

154 **3. Results**

155

156 In the four CM chondrites surveyed in this work, calcite grains surrounded by Fe-S-
157 rich serpentine/tochilinite (hereafter T1 calcite; Fig. 1a) are ubiquitous whereas serpentine-
158 free polycrystalline calcite grains containing Fe-Ni sulfide inclusions (hereafter T2 calcite;
159 Fig. 1b) have only been observed in two sections (Jbilet Winselwan and Mukundpura). The O
160 isotopic compositions of T1 calcite grains measured herein vary widely, with $\delta^{18}\text{O}$ values
161 ranging from 23.1 to 44.3‰, $\delta^{17}\text{O}$ from 11.1 to 23.4‰ and $\Delta^{17}\text{O}$ from -2.8 to $+1.8\text{‰}$ (Figs 1c
162 & S1, Table S1), whereas T2 calcite grains have homogeneous compositions with $\delta^{18}\text{O}$ values
163 ranging from 12.6 to 18.4‰, $\delta^{17}\text{O}$ from 4.2 to 8.1‰ and $\Delta^{17}\text{O}$ from -4 to -0.8‰ (Figs 1c &
164 S1, Table S2)



165

166 **Fig. 1:** Backscattered electron images of (a) a T1 calcite grain (Cal) surrounded by a Fe-S-rich
 167 Serpentine/Tochilinite rim (Srp/Tch) in the matrix of Murchison and (b) a T2 calcite grain that is free of
 168 serpentine/tochilinite rim, but is instead surrounded by a rim of Fine-Grained Matrix (FGR; white dashed
 169 line) in the matrix of Mukundpura. White circles represent the locations of SIMS analytical spots. (c) $\delta^{17}\text{O}$ -
 170 $\delta^{18}\text{O}$ plot for T1 (circles) and T2 (diamonds) calcites from the CM chondrites Maribo (black), Murchison
 171 (green), Jbilet Winselwan (orange) and Mukundpura (red) (2σ errors). Schematic $\delta^{17}\text{O}$ - $\delta^{18}\text{O}$ diagrams
 172 represent the linear correlations (black solid lines) obtained considering (d) T1 and T2 calcites, defining a
 173 mass-independent trend with a slope of 0.61 ± 0.03 and (e) only T1 calcites, defining a mass-dependent
 174 trend with a slope of 0.53 ± 0.06 . TFL = Terrestrial Fractionation Line ($\delta^{17}\text{O} = 0.52 \times \delta^{18}\text{O}$); PCM =
 175 Primary Chondrule Minerals line ($\delta^{17}\text{O} = 0.987 \times \delta^{18}\text{O} - 2.7$).

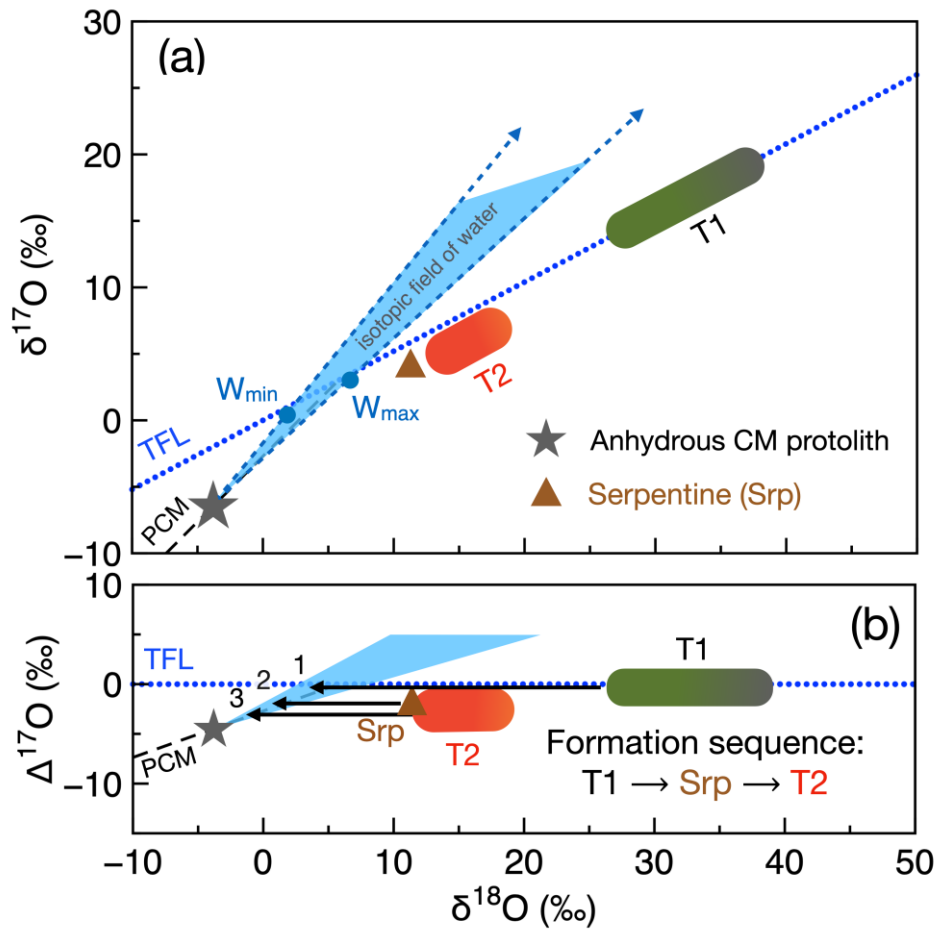
176 4. Discussion

177

178 Together, T1 and T2 calcite grains define a mass-independent trend with $\delta^{17}\text{O} = (0.61$
179 $\pm 0.03) \times \delta^{18}\text{O} - (3.3 \pm 1.1)$ (Fig. 1c–d) that is similar, within errors, to those commonly
180 reported in different CM chondrites (Vacher et al. 2018). As a first approximation, this trend
181 suggests that the O isotopic compositions of CM carbonates is essentially controlled by
182 variable degrees of isotopic exchanges between ^{16}O -rich anhydrous silicates and a $^{17,18}\text{O}$ -rich
183 fluid (Fig. 1d; Verdier-Paoletti et al. 2017; Marrocchi et al. 2018). However, the O isotopic
184 compositions of T1 calcites alone define a distinct trend with $\delta^{17}\text{O} = (0.53 \pm 0.06) \times \delta^{18}\text{O} -$
185 (1.2 ± 2.2) that is indistinguishable, within errors, from the TFL (i.e., $\Delta^{17}\text{O} = -0.4 \pm 1.0$; Fig.
186 1e). Conversely, T2 calcites exhibit clustered $\delta^{17}\text{O} - \delta^{18}\text{O}$ values (Figs 1c & S1, Table S2)
187 with $\Delta^{17}\text{O} = -2.6 \pm 1.0$, which artificially produce the aforementioned mass-independent
188 trend when taken together with T1 calcites (Fig. 1d). This demonstrates that petrographic
189 observations of carbonates are essential for understanding the O isotopic evolution of
190 asteroidal fluids and the constraints they bear.

191 Based on mass-balance calculations, tentative attempts at estimating the O isotopic
192 composition of primordial water accreted by CM chondrites have led to widely ranging and
193 contrasted results due to assumptions on the O isotopic composition of the anhydrous
194 protolith and asteroidal thermal evolution ($\delta^{18}\text{O}_{\text{fluid}} = 16\text{--}55\text{‰}$, $\delta^{17}\text{O}_{\text{fluid}} = 9\text{--}35\text{‰}$ and
195 $\Delta^{17}\text{O}_{\text{fluid}} = 0.9\text{--}6.6\text{‰}$; Verdier-Paoletti et al. 2017; Clayton & Mayeda 1999; Fujiya 2018).
196 However, these values correspond to the initial water composition and do not represent the
197 oxygen isotopic compositions of fluids from which carbonates precipitated, which had Earth-
198 like compositions with $\Delta^{17}\text{O} \approx 0\text{‰}$ (Fig. 1c; Vacher et al. 2016; Verdier-Paoletti et al. 2017).
199 Quantitative estimates of the O isotopic compositions of the parental fluids of carbonates have
200 been obtained by CO_2 clumped-isotope thermometry (Δ^{47} ; Guo & Eiler 2007), which

201 corresponds to anomalous enrichments of mass 47 (i.e., $^{13}\text{C}^{18}\text{O}^{16}\text{O}$) in CO_2 derived from
202 H_3PO_4 digestion of carbonates (Ghosh et al. 2006). Based on measurements performed on the
203 CM chondrites Murchison and Murray, dominated by T1 calcites, Guo & Eiler (2007)
204 estimated that the O isotopic compositions of their alteration fluids ranged from $\delta^{18}\text{O} = 2\text{‰}$
205 and $\Delta^{17}\text{O} = -0.6\text{‰}$ (hereafter W_{min} ; Fig. 2a) to $\delta^{18}\text{O} = 6.8\text{‰}$ and $\Delta^{17}\text{O} = -0.5\text{‰}$ (hereafter
206 W_{max} ; Fig. 2a). Because these fluids experienced oxygen isotopic exchanges with the
207 anhydrous CM chondrite protolith ($\delta^{18}\text{O} = -3.8\text{‰}$, $\delta^{17}\text{O} = -6.5\text{‰}$; Fig. S2), they define two
208 trends that delimit the possible O isotopic compositions of CM alteration fluids (blue shaded
209 area in Fig. 2a). Considering these extreme trends, the precipitation temperatures of each T1
210 calcite grain can be calculated according to the isotopic fractionation factor α (Watkins et al.
211 2013), which corresponds to the distance between the minimum and maximum trends and the
212 O isotopic compositions of carbonates in the three oxygen isotope diagram. This estimation
213 leads to respective minimum (T_{min}) and maximum (T_{max}) precipitation temperatures of $-9 \pm$
214 11 °C and $5 \pm 14 \text{ °C}$ for Maribo, $19 \pm 22 \text{ °C}$ and $50 \pm 34 \text{ °C}$ for Murchison, $15 \pm 21 \text{ °C}$ and 33
215 $\pm 29 \text{ °C}$ for Jbilet Winselwan and $12 \pm 17 \text{ °C}$ and $34 \pm 22 \text{ °C}$ for Mukundpura (1σ ; Table 1
216 and Fig. 3a). On average, this gives minimum and maximum precipitation temperatures for all
217 T1 calcites of $7 \pm 22 \text{ °C}$ and $29 \pm 32 \text{ °C}$, respectively (1σ).



218

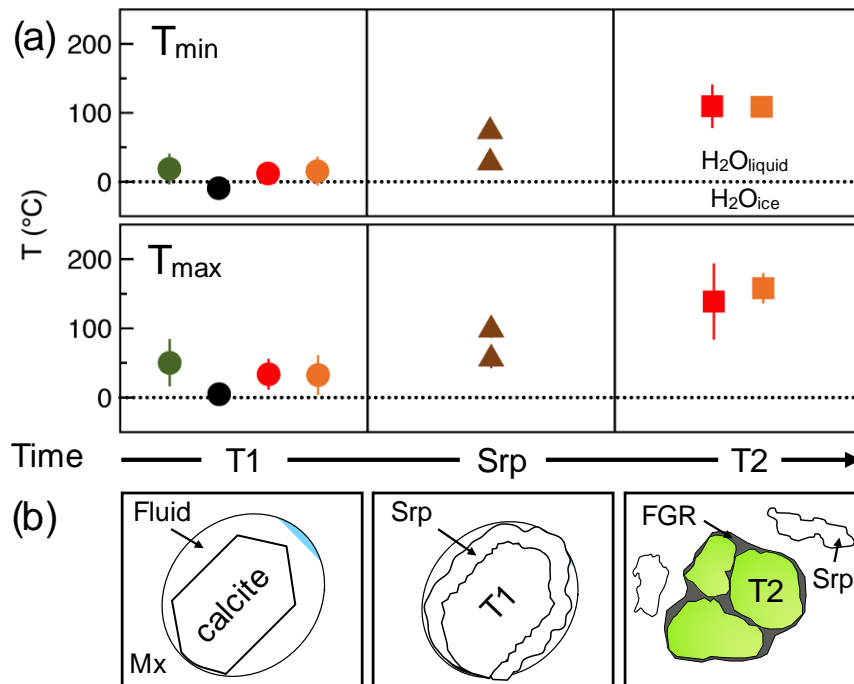
219 **Fig. 2:** (a) $\delta^{17}\text{O}$ - $\delta^{18}\text{O}$ plot showing simplified ranges for T1 and T2 calcites, the mean bulk value of CM
 220 serpentine (Srp, brown triangle) and the isotopic field of CM water (blue shaded area) as determined from
 221 the isotopic equilibration (blue dashed lines) of the minimum (W_{\min}) and maximum (W_{\max}) compositions of
 222 the parental water of T1 calcites (blue circles) with the anhydrous CM protolith (grey star; see
 223 Supplementary Fig. S1 for details). (b) $\delta^{18}\text{O}$ - $\Delta^{17}\text{O}$ plot showing the isotopic equilibration of CM water with
 224 the anhydrous CM protolith. In this diagram, mass-dependent isotopic fractionations plot on a horizontal
 225 line. The decrease of the mean $\Delta^{17}\text{O}$ values of the secondary phases ($\Delta^{17}\text{O}_{\text{T1}} = 0.4\text{‰}$, $\Delta^{17}\text{O}_{\text{Srp}} = -2.2\text{‰}$ and
 226 $\Delta^{17}\text{O}_{\text{T2}} = -2.4\text{‰}$; see Supplementary Tables S1 and S2 and Clayton & Mayeda 1999) indicates the
 227 following formation sequence: (1) T1 calcites, (2) serpentines and (3) T2 calcites.

228

229 **Table 1:** Mean O isotopic compositions of secondary phases and their calculated minimum (T_{\min}) and
 230 maximum (T_{\max}) formation temperatures (O'Neil et al., 1969). Uncertainties are 1σ .
 231

Meteorite	Petrologic subtype	Secondary phase	Sample number	Mean $\delta^{18}\text{O}$ (‰)	Mean $\Delta^{17}\text{O}$ (‰)	Mean T_{\min} (°C)	Mean T_{\max} (°C)
Maribo	CM2.6/2.7 ^a	T1 calcite	25	38.3 (± 3.1)	-1.2 (± 0.5)	-9 (± 11)	5 (± 14)
Murchison	CM2.5 ^b	T1 calcite	24	33.7 (± 4.5)	0.4 (± 0.8)	19 (± 22)	50 (± 34)
Jbilet	CM2.4/2.7 ^c	T1 calcite	10	31.4 (± 4.1)	-1.6 (± 1.2)	15 (± 21)	33 (± 29)
Winselwan		T2 calcite	2	17.5 (± 0.6)	-1 (± 0.3)	109 (± 11)	158 (± 22)
Mukundpura	CM2.0 ^d	T1 calcite	8	33.5 (± 3.8)	-0.7 (± 0.6)	12 (± 17)	34 (± 22)
		T2 calcite	13	15.4 (± 2)	-2.6 (± 1)	110 (± 32)	139 (± 55)
Bulk CM	–	Serpentine ^e	5	11.7 (± 0.6)	-2.2 (± 0.3)	28 (± 8) ^f 73 (± 7) ^g	56 (± 13) ^f 98 (± 11) ^g

232 References: ^a(van Kooten et al. 2018); ^b(Rubin et al. 2007); ^c(King et al. 2018); ^d(Rudraswami
 233 et al. 2018); ^e(Clayton & Mayeda 1999); ^f(Früh-Green et al. 1996); ^g(Zheng 1993)
 234



235
 236 **Fig. 3:** (a) Minimum (T_{\min}) and maximum (T_{\max}) precipitation temperatures of T1 calcites (circles),
 237 serpentines (brown triangles) and T2 calcites (diamonds) calculated as a function of their formation
 238 sequence/time (errors are 1σ) using previously reported fractionation factors for calcite (O'Neil et al.,
 239 1969) and serpentine (Früh-Green et al. 1996; Zheng 1993). Colours are as in Fig. 1. (b) Schematic
 240 representation of the formation sequence of (1) T1 calcite, (2) serpentine around T1 calcite and (3) T2
 241 calcite, as deduced from petrographic observations and the mean $\Delta^{17}\text{O}$ values of these three phases (see
 242 Fig. 2c).
 243

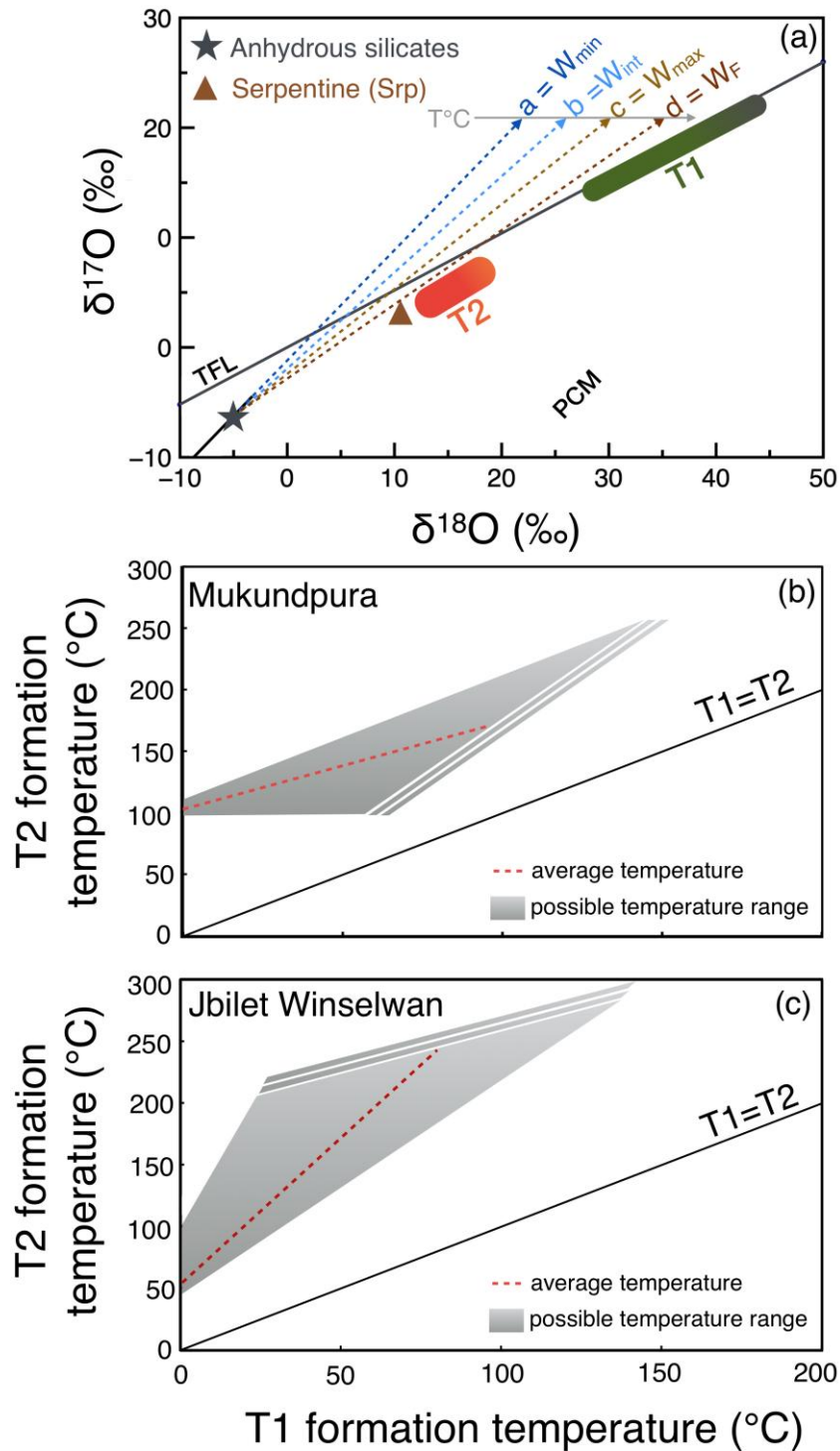
244 The large range of $\delta^{17}\text{O}$ - $\delta^{18}\text{O}$ values and constant $\Delta^{17}\text{O}$ values observed in T1 calcites
245 (Fig. 1c–e, Table S1) imply that T1 calcites precipitated along a temperature gradient from
246 alteration fluids characterized by a fixed $\Delta^{17}\text{O}$ value. On the other hand, T2 calcites (this
247 study) and serpentine (Clayton & Mayeda 1984) formed from a more ^{16}O -rich fluid that
248 resulted from protracted isotopic exchange with the ^{16}O -rich anhydrous protolith and thus
249 evolved toward negative $\Delta^{17}\text{O}$ values (Fig. 2b). Following the same methodology as for T1
250 calcites, we calculated the formation temperatures of T2 calcites to be significantly higher,
251 with respective minimum and maximum temperatures being 109 ± 11 °C and 158 ± 22 °C for
252 Jbilet Winselwan and 110 ± 11 °C and 139 ± 55 °C for Mukundpura (1σ ; Table 1 and Fig.
253 3a); respective average values are 109 ± 29 °C and $141^\circ\text{C} \pm 52^\circ\text{C}$ (1σ). The same calculation
254 for bulk serpentine compositions ($n = 5$; Clayton & Mayeda 1999) gives minimum and
255 maximum formation temperatures of 28 ± 8 to 56 ± 13 °C and 73 ± 7 to 98 ± 11 °C,
256 respectively, depending of the fractionation factor considered (Früh-Green et al. 1996; Zheng
257 1993; 1σ ; Table 1 and Fig. 3a).

258 Our petrographic and isotopic approaches reveal that T1 calcites precipitated at lower
259 temperatures than serpentines and T2 calcites (Fig. 3a). These results support petrographic
260 observations suggesting that T2 calcites correspond to a later stage of alteration, as
261 highlighted by (i) the absence of serpentine rims and (ii) the existence of a fine-grained rim
262 (FGR) suggesting that they replaced chondrule silicates (Fig. 3b; Lee et al. 2014; Lindgren et
263 al. 2017). This implies that fluid circulation in CM parent bodies, and thus the formation of
264 CM secondary phases, occurred during a prograde thermal evolution (Figs. 2b and 3b; Vacher
265 et al. 2019), with T1 calcites forming first at $T = -10$ to $+50$ °C, followed by the precipitation
266 of (Fe,S)-rich serpentine (mostly cronstedtite; Pignatelli et al. 2016; 2017) and tochilinite at T
267 $= 30$ – 100 °C and finally T2 calcites at $T = 110$ – 160 °C (Fig. 3a, Table 1).

268 According to X-ray diffraction studies (Howard et al. 2011; 2009), serpentine
269 represent the most abundant mineral in CM chondrites (75 vol% in average). Their formations
270 (posterior to that of T1 calcites) would thus affect the isotopic evolution of the alteration
271 fluids, leading to a slight shift toward ^{16}O -enriched values. As this isotopic shift is not taken
272 into account in our model, this implies that the precipitation temperatures estimated for T2
273 calcites (Fig. 3a, Table 1) should be considered as maximum values. However, as the
274 fractionation factor α is significantly lower for serpentine-water than for calcite-water (i.e.,
275 $1000\ln\alpha_{\text{serpentine-water}} = 6.3$ vs $1000\ln\alpha_{\text{calcite-water}} = 17.1$ at 100°C ; O'Neil et al. 1969; Fruh-
276 Green et al., 1996), this approximation does not affect our main conclusions that T1 calcites
277 precipitated at lower temperature than T2 calcites.

278 As the uncertainties on the O isotopic compositions of primordial water accreted by
279 CM chondrites could also affect our conclusions, we tested our results with different initial O
280 isotopic compositions (Fig. 4). According to the currently favoured self-shielding model,
281 primordial water is hypothesized to have had a large $^{17,18}\text{O}$ enrichment (i.e., $\delta^{17}\text{O} = \delta^{18}\text{O} \approx$
282 180% ; Sakamoto et al. 2007) plotting on a line of slope 1 in a three oxygen isotope diagram.
283 However, mass balance calculations performed on the O isotopic compositions of CM
284 chondrites at bulk and mineral scales suggest more modest enrichments in the heavy oxygen
285 isotopes with $\delta^{17}\text{O} = 35 \pm 9\%$ and $\delta^{18}\text{O} = 55 \pm 13\%$ (Fujiya 2018). Hence, we tested our
286 results by using primordial CM water O isotopic compositions corresponding to (i) a
287 composition intermediate between W_{\min} and W_{\max} (W_{int}) and (ii) the values proposed by
288 Fujiya (2018) (W_{F} , Fig. 4a). Isotopic exchange between these fluid compositions and the
289 anhydrous CM protolith (Marrocchi et al. 2018) thus defines two other lines on the $\delta^{17,18}\text{O}$
290 diagram (b and d in Fig. 4a, with lines a and c corresponding to the trends defined by W_{\min}
291 and W_{\max} , respectively) from which the precipitation temperatures of T1 and T2 calcites can
292 be calculated according to the fractionation factor α (Watkins et al. 2013). The results for

293 Jbilet Winselwan and Mukundpura (the only meteorites containing T2 calcites in this study)
294 systematically show that T2 calcites precipitated at higher temperatures than T1 calcites (Fig.
295 4b–c), regardless of the oxygen isotopic composition used for primordial water. Depending
296 on the isotopic trend considered (a, b, c or d in Fig. 4a), the average precipitation temperatures
297 of T1 calcites range from 10 to 100 °C, whereas T2 calcites formed between 110 and 245 °C
298 (Fig. 4b–c). We note that the absolute temperatures at which secondary phases formed is
299 directly affected by the oxygen isotopic composition of primordial chondritic water, whose
300 precise determination is thus fundamental to better quantifying the thermal evolution of
301 hydrated asteroids.



302

303 **Fig. 4:** (a) $\delta^{17}\text{O}$ - $\delta^{18}\text{O}$ plot showing the four trends (see text) used to calculate the influence of the initial
 304 oxygen isotopic composition of primordial water on the thermal path interpreted for water-rich asteroids.
 305 (b, c) $\delta^{17}\text{O}$ - $\delta^{18}\text{O}$ plots showing the results of the model for Mukundpura and Jbilet Winselwan, respectively.
 306 In both cases, the average formation temperatures of T2 calcites are systematically higher than those
 307 estimated for T1 calcites (red dashed lines), even when accounting for variability in the $\delta^{17}\text{O}$ and $\delta^{18}\text{O}$
 308 values of calcites in Jbilet Winselwan and Mukundpura (grey triangles).

309

310 Another possible source of uncertainty in estimating precipitation temperatures arises
311 if T1 calcites experienced post-precipitation isotopic reequilibration, especially if CM
312 chondrites experienced peak temperatures as high as 250 °C. However, this appears unlikely
313 as T1 calcites systematically show mass-dependent oxygen isotopic variations
314 (Supplementary Fig. S3), whereas isotopic exchange between initial water and anhydrous
315 silicates during reequilibration would have induced $\Delta^{17}\text{O}$ variations (Fig. 2a). In addition,
316 according to the values of oxygen self-diffusion in calcite (Anderson 2007; Farver 1994), 1–
317 10^4 Gyr are required to isotopically reequilibrate calcite grains of 5 μm in size at temperatures
318 ≤ 200 °C (Fig. S3). Such results thus strengthen our conclusion that hydrated asteroids
319 experienced a prograde thermal evolution with T1 calcites precipitating first, followed by
320 serpentine and then T2 calcites.

321 By taking into account the petrographic type of carbonates, our hydrothermal
322 temperature estimates for CM chondrites are higher than previously proposed (Clayton &
323 Mayeda 1984; Benedix et al. 2003; Guo & Eiler 2007) but remain low (< 250 °C) compared to
324 the peak of thermal metamorphism experienced by other groups of carbonaceous chondrites,
325 such as CO or CV chondrites (up to 500–600 °C; Bonal et al. 2007; Busemann et al. 2007;
326 Cody et al. 2008; Ganino & Libourel 2017). This implies the relatively late accretion of
327 water-rich asteroids in the protoplanetary disk, as water-poor asteroids that accreted earlier
328 experienced significantly higher temperatures due to the radioactive decay of ^{26}Al . Based on
329 $\epsilon^{54}\text{Cr}$ anomalies, it has been proposed that CM chondrites accreted ~ 3.7 – 5.0 Myr after the
330 formation of CV calcium-aluminium-rich inclusions (CAIs; Fujiya et al. 2012; Doyle et al.
331 2015; Sugiura & Fujiya 2014), after a five-fold decrease in the abundance of ^{26}Al , whereas
332 CO and CV chondrites accreted ~ 2.1 – 2.4 and ~ 2.4 – 2.6 Myr after CV CAIs, respectively
333 (Doyle et al. 2015). Interestingly, recent spectral data provided by the Osiris-REx and
334 Hayabusa2 asteroid sample return missions suggest that C-type asteroid Ryugu has

335 experienced more heating than B-type asteroid Bennu (Hamilton et al. 2019; Kitazato et al.,
336 2019). Although late shock heating could have induced such features, their different thermal
337 history could also be the result of distinct accretion ages. The returned samples from Osiris-
338 REx and Hayabusa2 in the near future will likely contain hydrated minerals (Kitazato et al.
339 2019; Lauretta et al. 2019) whose *in-situ* isotopic analyses would provide information on the
340 thermal alteration processes and formation histories of asteroids Ryugu and Bennu.

341

342 **5. Conclusions**

343

344 In this letter, we report the results of *in-situ* oxygen isotope analyses performed on
345 alteration phases (calcium carbonates) from a suite of different hydrated meteorites (CM
346 chondrites) to quantitatively estimate the thermal evolution of hydrated asteroids. Based on our
347 isotopic results, we propose a new isotopic model that reconciles formation temperatures and
348 petrographic observations of secondary minerals whose isotopic compositions recorded a
349 gradual increase of the temperature (up to 250°C) during a prograde evolution of the
350 temperature, regardless the oxygen isotopic composition of the initial water. These results are
351 fundamental because they imply that hydrated asteroids accreted relatively late in the
352 protoplanetary disk, as their earlier accretion would have led to higher alteration temperatures
353 due to higher concentrations of radioactive ^{26}Al . Although more precise radioactive dating
354 and numerical modelling are required, our study provides a key method to quantitatively
355 estimate the respective thermal histories of the asteroids Bennu (Lauretta et al. 2019) and
356 Ryugu (Sugita et al. 2019; Watanabe et al. 2019) upon the return of samples to Earth.

357

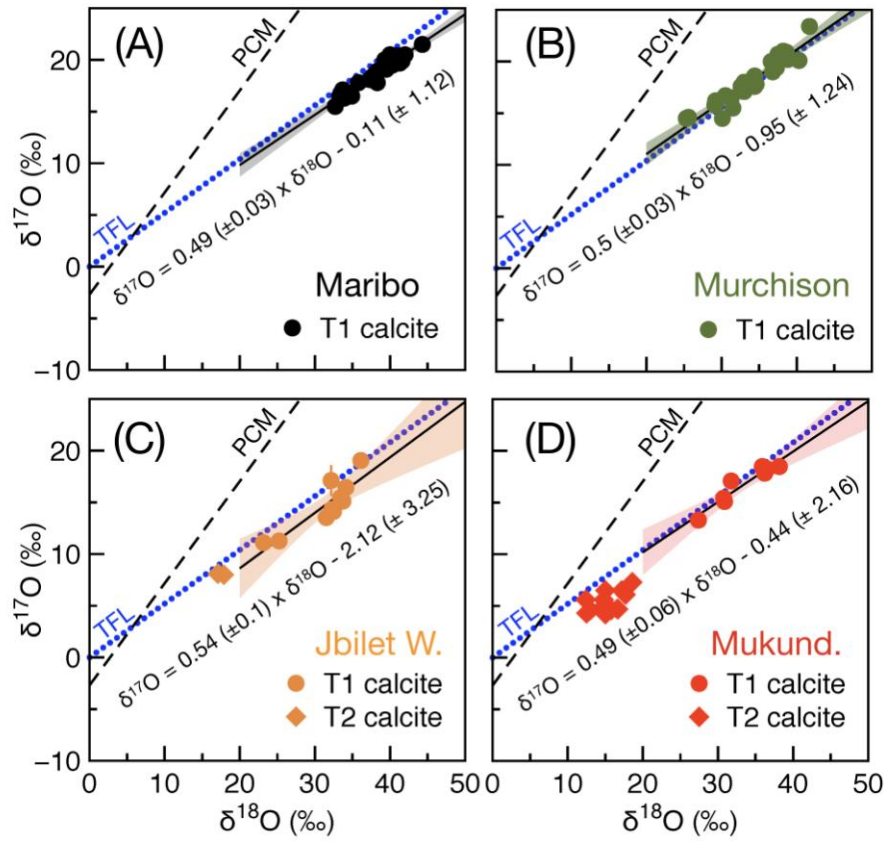
358

359 **Acknowledgments**

360

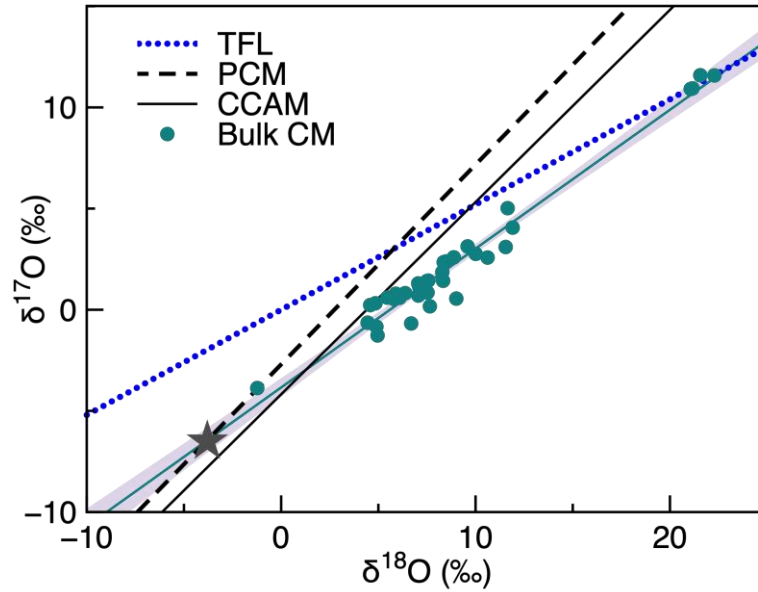
361 The authors are grateful to Nordine Bouden and Johan Villeneuve for their assistance
362 with the isotopic measurements. Laurette Piani is thanked for helpful scientific discussions.

363 The Muséum National d'Histoire Naturelle (Paris) and The Natural History Museum of
364 Denmark (Copenhagen) are also thanked for providing samples of Mukundpura and sections
365 of Maribo chondrites. We thank Pr. Frederic Rasio for his editorial handling and the
366 anonymous reviewer for his comments that contributed to improve the quality of the
367 manuscript. This research was funded by l'Agence Nationale de la Recherche through grant
368 ANR-587 14-CE33-0002-01 SAPINS (PI Yves Marrocchi). This is CRPG contribution #2714.
369



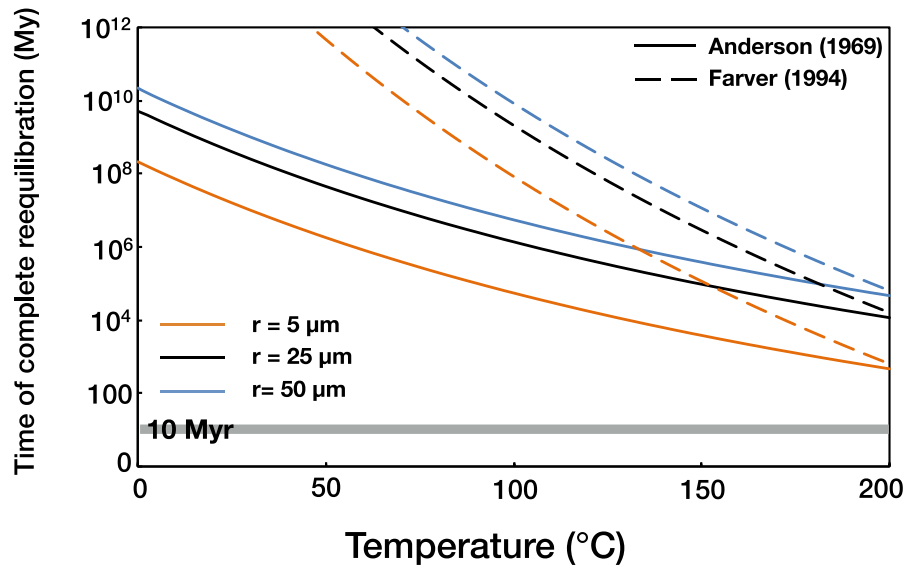
372
 373 **Fig. S1:** $\delta^{17}\text{O}$ - $\delta^{18}\text{O}$ plots showing the mass-dependent trends (black solid line) defined by T1 calcites
 374 (circles) for each CM chondrite: (a) Maribo, (b) Murchison, (c) Jbilet Winselwan and (d) Mukundpura.
 375 Shaded areas represent the 95% confidence interval for each slope. T2 calcites (diamonds) are also shown
 376 for Jbilet Winselwan (c) and Mukundpura (d), the only chondrites studied herein containing T2 calcites.
 377 Errors are 2σ .

378
 379
 380
 381
 382



383
 384 **Fig. S2:** $\delta^{17}\text{O}$ - $\delta^{18}\text{O}$ plot showing the O isotopic composition of the anhydrous CM protolith (i.e., the
 385 theoretical anhydrous bulk CM composition: $\delta^{18}\text{O} = -3.8\text{‰}$ and $\delta^{17}\text{O} = -6.5\text{‰}$; grey star) determined from
 386 the linear correlation of the CM bulk composition (green circle (Clayton & Mayeda 1999; Hewins et al.
 387 2014)). The anhydrous CM protolith corresponds to the intercept between the bulk CM trend ($\delta^{17}\text{O} = 0.69$
 388 $\times \delta^{18}\text{O} - 3.8$; $n = 36$) and the PCM line ($\delta^{17}\text{O} = 0.987 \times \delta^{18}\text{O} - 2.7$; (Ushikubo et al. 2012)). CCAM:
 389 Carbonaceous chondrite anhydrous minerals line.

390
 391
 392
 393
 394
 395
 396
 397
 398



399
 400
 401
 402
 403
 404
 405
 406
 407
 408
 409
 410
 411
 412
 413
 414
 415
 416
 417
 418
 419
 420
 421
 422
 423

Fig. S3: Time (Myr) required for the complete reequilibration of early precipitated T1 calcite as a function of grain size (radius) and temperature, calculated using oxygen self-diffusion parameters for calcite (Farver 1994). The grey shaded region at 10 Myr corresponds to the duration estimated for fluid circulations in asteroidal parent bodies (Fujiya et al. 2012; Doyle et al. 2015; Petit et al. 2011).

Table S1: Oxygen isotopic compositions of T1 calcite grains in the CM chondrites Maribo, Murchison, Jbilet Winselwan and Mukundpura.

#	$\delta^{18}\text{O}$	2σ	$\delta^{17}\text{O}$	2σ	$\Delta^{17}\text{O}$	2σ
CC7	32.7	0.3	15.5	0.5	-1.5	0.8
CC21-1	33.3	0.3	16.5	0.8	-0.8	1
CC21-2	33.9	0.3	16.3	0.7	-1.3	0.9
CC22	33.7	0.3	17.1	0.5	-0.4	0.8
CC20	34.1	0.4	16.9	0.6	-0.9	0.9
CC27	34.9	0.2	16.5	0.5	-1.7	0.7
CC30	35.8	0.3	17.8	0.5	-0.8	0.7
CC10	37.3	0.6	18.1	0.6	-1.3	1
CC11	37.7	0.2	18.4	0.5	-1.3	0.7
CC4-2	38	0.3	18.6	0.5	-1.1	0.8
CC4-1	41.6	0.3	19.9	0.5	-1.7	0.7
CC5	38.3	0.3	18.9	0.6	-1.1	0.8
CC17	38.3	0.3	17.8	0.6	-2.2	0.8
CC9	39.3	0.3	20	0.5	-0.4	0.8
CC33	39.5	0.3	19.1	0.5	-1.4	0.5
CC32	39.5	0.3	19.6	0.7	-0.9	0.9
CC13	40	0.5	20.5	0.6	-0.3	1
CC3	40.2	0.3	20	0.6	-0.9	0.7
CC28	40.3	0.2	19.5	0.6	-1.4	0.8
CC29	40.5	0.3	19.6	0.6	-1.5	0.6
CC12	40.6	0.3	19.7	0.5	-1.4	0.8
CC15	40.9	0.4	20.4	0.5	-0.9	0.6
CC2	41.3	0.3	19.7	0.5	-1.7	0.8
CC18	42	0.3	20.5	0.5	-1.4	0.8
CC1	44.3	0.3	21.5	0.6	-1.5	0.8
Mean	38.3		18.7		-1.2	
<i>StDev</i>	<i>3.1</i>		<i>1.6</i>		<i>0.5</i>	
CC-7-2	25.3	0.2	14.5	0.4	1.3	0.3
CC-7-3	25.6	0.2	14.6	0.4	1.3	0.4
A-CC-5-2	29.1	0.5	15.8	0.4	0.7	0.6
A-CC-5-3	36.6	0.2	20	0.3	1	0.3
A-CC-8-2	29.2	0.6	15.9	0.6	0.7	0.7
CC-1-2	29.2	0.3	16.2	0.4	1	0.4
A-CC-11-1	30.1	0.5	14.5	0.6	-1.1	0.7
CC-6	30.5	0.3	16.7	0.3	0.8	0.4
A-CC-3-2	31.3	0.9	16.5	0.8	0.3	1.1
A-CC-3-1	34.4	0.7	18.6	0.7	0.7	0.9
A-CC-10	31.5	0.9	15.5	0.6	-0.9	1.0
A-CC-13	32.6	0.3	17.6	0.3	0.7	0.4
A-CC-7	33	0.5	17.1	0.6	0	0.7
CC-18	33	0.2	18	0.3	0.9	0.3
A-CC-2-2	34.4	0.6	17.6	0.6	-0.3	0.8
CC-3	34.6	0.3	17.8	0.4	-0.2	0.4
CC-2	36.8	0.2	19	0.3	-0.1	0.3
CC-5	37.3	0.6	19.4	0.6	0	0.8
CC-10	37.5	0.2	20.7	0.3	1.2	0.3
CC-12	38.2	0.3	21	0.3	1.1	0.3
A-CC-1	38.6	0.6	20.9	0.6	0.8	0.8
CC-11	38.8	0.3	20.2	0.3	0	0.4
CC-9	40.3	0.3	20.1	0.3	-0.8	0.4
CC-8	41.7	0.4	23.4	0.3	1.8	0.4
Mean	33.7		18		0.4	
<i>StDev</i>	<i>4.5</i>		<i>2.4</i>		<i>0.8</i>	
CC-6	23.1	0.7	11.1	0.8	-0.9	1.0
CC-5	25.2	0.4	11.3	0.7	-1.9	0.7
CC-11	31.5	0.5	13.5	0.8	-2.8	0.9

CC-3	32.2	0.7	17.1	1.5	0.4	1.6
CC-2	32.3	0.6	14.3	0.7	-2.4	0.8
CC-7	32.5	0.5	14.1	0.7	-2.8	0.7
CC-9	33.4	0.5	15.4	0.7	-1.9	0.7
CC-8	33.7	0.5	15.1	0.8	-2.4	0.8
CC-1	34.1	0.5	16.4	0.7	-1.3	0.8
CC-10	36.1	0.5	19.1	0.8	0.3	0.8
Mean	31.4		14.8		-1.6	
<i>StDev</i>	<i>4.1</i>		<i>2.5</i>		<i>1.2</i>	
CC15	27.4	0.7	13.3	0.4	-0.9	0.6
CC13	30.8	0.6	15.4	0.4	-0.6	0.6
CC14	30.9	0.6	15.1	0.4	-1	0.6
CC1	31.8	0.5	17.1	0.4	0.6	0.5
CC12	35.9	0.6	18.5	0.4	-0.2	0.6
CC8-1	36.2	0.6	17.8	0.4	-1	0.6
CC11	36.5	0.6	18.2	0.4	-0.8	0.6
CC7-1	38.2	0.6	18.5	0.4	-1.4	0.6
Mean	33.5		16.7		-0.7	
<i>StDev</i>	<i>3.8</i>		<i>1.9</i>		<i>0.6</i>	

Shaded rows denote multiple analyses of the same grain.

426
427
428
429
430
431
432
433
434
435
436
437
438
439
440
441
442
443
444
445
446
447
448
449
450
451
452
453
454
455
456
457
458
459
460

461 **Table S2:** Oxygen isotopic compositions of T2 calcite grains in the CM chondrites Jbilet Winselwan and
 462 Mukundpura.

#	$\delta^{18}\text{O}$	2σ	$\delta^{17}\text{O}$	2σ	$\Delta^{17}\text{O}$	2σ
CC15	17.1	0.4	8.1	0.9	-0.8	0.9
CC14	17.9	0.5	8	0.8	-1.3	0.0
Mean	17.5		8.1		-1	
<i>StDev</i>	<i>0.6</i>		<i>0</i>		<i>0.3</i>	
CC3-1	12.4	0.6	5.6	0.3	-0.9	0.5
CC3-4	12.5	0.6	4.3	0.4	-2.2	0.6
CC3-3	13	0.6	4.6	0.4	-2.2	0.6
CC3-2	15	0.5	6.5	0.4	-1.2	0.6
CC17-1	14.7	0.6	4.9	0.4	-2.7	0.6
CC17-2	17.7	0.6	6.1	0.4	-3.1	0.6
CC5-1	14.8	0.7	5.6	0.4	-2	0.6
CC5-5	15	0.8	4.2	0.5	-3.6	0.7
CC5-3	15.8	0.7	4.6	0.4	-3.6	0.7
CC5-2	16.6	0.5	4.7	0.4	-3.9	0.5
CC5-4	16.7	0.6	4.7	0.5	-4	0.6
CC6-1	17.2	0.6	6.5	0.4	-2.5	0.6
CC9	18.6	0.8	7.3	0.4	-2.4	0.7
Mean	15.4		5.4		-2.6	
<i>StDev</i>	<i>2.0</i>		<i>1.0</i>		<i>1.0</i>	

Shaded rows denote multiple analyses of the same grain.

463
 464
 465
 466
 467
 468
 469
 470
 471
 472
 473
 474
 475
 476
 477
 478
 479
 480
 481
 482
 483
 484
 485
 486
 487
 488
 489
 490
 491
 492
 493

494 **References**

- 495 Alexander, C. M. O., Bowden, R., Fogel, M. L., & Howard, K. T. 2015, *MPS*, 50, 810.
- 496 Anderson, T. F. 1969, *J. Geophys. Res.*, 74, 3918.
- 497 Benedix, G. K., Leshin, L. A., Farquhar, J., Jackson, T., et al 2003, *GCA*, 67, 1577.
- 498 Bonal, L., Bourot-Denise, M., Quirico, E., et al. 2007, *GCA*, 71, 1605.
- 499 Brearley, A. J. 2006, *MESS II*, 943, 587.
- 500 Briani, G., Gounelle, M., Bourot-Denise, M., & Zolensky, M. E. 2012, *MPS*, 47, 880.
- 501 Burbine, T., McCoy, T., Meibom, A., Gladman, B., & Keil, K. 2002, *Asteroids III*, 1, 653.
- 502 Busemann, H., Alexander, C. M. O'D., & Nittler, L. R. 2007, *MPS*, 42, 1387.
- 503 Clayton, R. N., & Mayeda, T. K. 1984, *EPSL*, 67, 151.
- 504 Clayton, R. N., & Mayeda, T. K. 1999, *GCA*, 63, 2089.
- 505 Cody, G. D., Alexander, C. M. O'D., Yabuta, H., et al. 2008, *EPSL*, 272, 446.
- 506 Doyle, P.M., Jogo, K., Nagashima, K., et al. 2015, *Nat Comms* 6, 7444.
- 507 Farver, J.R. 1994, *EPSL*, 121, 575.
- 508 Früh-Green, G. L., Plas, A., Lécuyer C. 1996, 14. *Proc. Ocean Drilling. Programm.* 147, 255.
- 509 Fuchs, L. H., Olsen, E., & Jensen, K. J. 1973, *Smithsonian Contr. Earth Sci.*, 10, 1.
- 510 Fujiya, W., Sugiura, N., Hotta, H., et al. 2012, *Nat Comms*, 3, 627.
- 511 Fujiya, W., Sugiura, N., Marrocchi, Y., et al. 2015, *GCA*, 161, 101.
- 512 Fujiya, W. 2018, *EPSL*, 481, 264.
- 513 Ganino, C., Libourel, G. 2017 *Nat Comms*, 8, 261.
- 514 Ghosh, P., Adkins, J., Affek, H., et al. 2006, *GCA*, 70, 1349.
- 515 Guo, W., & Eiler, J. M. 2007, *GCA*, 71, 5565.
- 516 Hamilton, V. E., Simon, A. A., Christensen, P. R., et al. 2019, *Nat. Astron.*, 3, 332.
- 517 Hewins, R. H., Bourot-Denise, M., Zanda, B., et al. 2014, *GCA*, 124, 190.
- 518 Hiroi, T., Pieters, C. M., Zolensky, M. E., & Lipschutz, M. E. 1996, *MPS*, 31, 321.
- 519 Howard, K. T., Benedix, G. K., Bland, P. A., & Cressey, G. 2009, *GCA*, 73, 4576.
- 520 Howard, K. T., Benedix, G. K., Bland, P. A., & Cressey, G. 2011, *GCA*, 75, 2735.
- 521 King, A. J., Russell, S. S., Schofield, P. F., et al. 2018, *MPS*, 49, 62.
- 522 Kitazato, K., Milliken, R. E., Iwata, T., et al. 2019, *Science*, 364, 272.
- 523 Lauretta D.S., DellaGiustina, D. N., Bennett, C. A., et al. 2019, *Nature*, 568, 55.
- 524 Lee, M. R., Sofe, M. R., Lindgren, P., Starkey, N. A., & Franchi, I. A. 2013, *GCA*, 121, 452.
- 525 Lee, M. R., Lindgren, P., & Sofe, M. R. 2014, *GCA*, 144, 126.
- 526 Lindgren, P., Lee, M. R., Starkey, N. A., Franchi, I. A. 2017, *GCA*, 204, 240.
- 527 Marrocchi, Y., Gounelle, M., Blanchard, I., et al., 2014, *MPS*, 49, 1232.
- 528 Marrocchi, Y., Bekaert, D. V., & Piani, L. 2018, *EPSL*, 482, 23.
- 529 O'Neil, J.R., Clayton, R.N. & Mayeda, T.K. 1969, *J. Chem. Phys.* 51, 5547.
- 530 Petitat, M., Marrocchi, Y., McKeegan, K. D., et al. 2011, *MPS*, 46, 275.
- 531 Piani, L., Yurimoto, H., & Remusat, L. 2018, *Nat. Astron.* 2, 317.
- 532 Pignatelli, I., Marrocchi, Y., Mugnaioli, E., et al. 2017, *GCA*, 209, 106.
- 533 Pignatelli, I., Marrocchi, Y., Vacher, et al. 2016, *MPS*, 51, 785.
- 534 Rubin, A. E., Trigo-Rodriguez, J. M., & Huber, H. 2007, *GCA*, 71, 2361.
- 535 Rudraswami, N. G., Naik, A. K., Tripathi, R. P., et al. 2018, *Geoscience Frontiers*, 1-10.
- 536 Sakamoto, N., Seto, Y., Itoh, S., et al. 2007, *Science*, 317, 231.
- 537 Sugita, S., Tatsumi, E., Okada, T., et al. 2019, *Science*, 364, eaaw0422.
- 538 Sugiura, N., Fujiya, W. 2014, *MPS*, 49, 772.
- 539 Ushikubo, T., Kimura, M., Kita, N. T., Valley, J. W. 2012, *GCA*, 90, 242.
- 540 Vacher, L. G., Marrocchi, Y., Verdier-Paoletti, M. J., Villeneuve, J., & Gounelle, M., 2016, *ApJ L*, 827, L1-6.
- 541 Vacher, L. G., Marrocchi, Y., Villeneuve, J., Verdier-Paoletti, M. J., & Gounelle, M., 2017, *GCA*, 213, 271.

- 544 Vacher, L. G., Marrocchi, Y., Villeneuve, J., Verdier-Paoletti, M. J., & Gounelle, M.,2018,
545 GCA, 239, 213.
- 546 Vacher, L. G., Truche, L., Faure, F., et al. 2019, MPS, 23, 237.
- 547 van Kooten, E. M. M. E., Cavalcante, L. L., Nagashima, K., et al. 2018, GCA, 79, 102.
- 548 Verdier-Paoletti, M. J., Marrocchi, Y., Avice, G., et al. 2017, EPSL, 458, 273.
- 549 Vilas, F. 1994, Icarus, 111, 456.
- 550 Vilas, F., & Gaffey, M. J. 1989, Science, 246, 790.
- 551 Watanabe, S., Hirabayashi, M., Hirata, N., et al 2019, Science, 364, 26.
- 552 Watkins, J. M., Nielsen, L. C., Ryerson, F. J., & DePaolo, D. J. 2013, EPSL, 375, 349.
- 553 Young, E. D., Zhang, K. K., & Schubert, G. 2003, EPSL, 213, 249.
- 554 Zolensky, M. E., Mittlefehldt, D. W., Lipschutz, M. E., et al. 1997, GCA, 61, 5099.
- 555 Zheng Y.-F. 1993, GCA, 57, 1079.